


Nonlocal vibrational and dissociative-attachment dynamics in $e^- + \text{HNCO}$ beyond a one-dimensional model

Jiří Trnka, Karel Houfek , and Martin Čížek 

*Faculty of Mathematics and Physics, Charles University, Institute of Theoretical Physics,
and V Holešovičkách 2, 18000 Prague, Czech Republic*

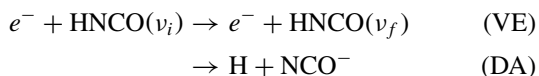
 (Received 17 April 2023; revised 6 October 2023; accepted 5 December 2023; published 10 January 2024)

We extend our previous calculations of the vibrational excitation and the dissociative electron attachment in the low-energy electron collisions with the HNCO molecule to include both stretching and bending modes in the motion of the hydrogen atom. These calculations confirm the assumption, made in our previous work, that the bending motion does not significantly alter the cross sections for the excitation of hydrogen stretching and dissociation. On the other hand, the extension of the model gives additional insight into the vibrational dynamics of the intermediate collision complex. We calculate the cross sections for the excitation of the hydrogen bending motion and we compare them with the recent experiments. The excitation curves for higher bending overtones show signs of interaction with the stretching motion. We also calculate the two-dimensional electron energy-loss spectrum within the model.

DOI: [10.1103/PhysRevA.109.012803](https://doi.org/10.1103/PhysRevA.109.012803)

I. INTRODUCTION

The main purpose of this paper is to extend our previous calculations of vibrational excitation (VE) and dissociative attachment (DA) processes in the electron collisions with the HNCO molecule [1,2]



by including more nuclear degrees of freedom and getting a better understanding of the dynamics.

The interest in electron scattering from HNCO molecules stems primarily from the fact that this molecule is abundant in interstellar space [3] and it has also been observed in cometary atmospheres [4]. It is also the smallest molecule containing the four most important elements forming biomolecules and could therefore be involved in the prebiotic chemistry [5,6] in space leading to the formation of important constituents of life, including amino acids. The studied processes may also serve as prototypes for understanding of similar reactions in larger molecules [7,8].

Cross sections for both dissociative electron attachment and the vibrational excitation of HNCO by collisions with electrons have been measured recently [1,2]. The DA cross section is characterized by sharp onset on the threshold at the electron energy of 1.16 eV followed by broad resonance with a maximum above 2 eV. The oscillatory structure between these two energies has been attributed to the opening of the vibrational excitation channels for the HN stretch. We have shown that all these features could be explained by the discrete-state-in-continuum model based on a resonance of mixed π^* and σ^* character [1]. The dynamics has been calculated within a one-dimensional model containing only

the NH stretch coordinate as a dynamical variable. The same model was used also in Ref. [2] to calculate the VE cross sections for one or two quanta of the NH stretch. The results of the one-dimensional calculation are in very good agreement with experiments, featuring sharp threshold peaks and Wigner cusps.

The success of these calculations to predict the experimental data suggests that the dynamics of the DA process proceeds basically in the direction of NH bond (see the geometry of the molecule schematically drawn in Fig. 1). On the other hand, the electron energy-loss spectra also show an excitation of other vibrational modes [2]. It is very difficult to treat the multimode dissociative attachment dynamics, but the successful one-dimensional (1D) model of the NH stretching dynamics may be a good starting point in the construction and testing of the multidimensional model of VE and DA processes that can be verified on the measurement of the excitation of other modes. This development is highly desirable for the understanding of systems where the coupling among several degrees of freedom may be even more important (see, for example, Refs. [7,9,10]).

The treatment of the vibrational dynamics in electron-molecule collisions in more vibrational degrees of freedom is highly nontrivial [11–14]. The calculations usually resort to the local complex potential (LCP) approximation that simplifies the numerical treatment significantly, but it is still very difficult even in the case of small polyatomic molecules [15–18]. On the other hand the LCP approximation is unable to describe the features originating from the interchannel coupling like the threshold peaks or Wigner cusps. The dynamics of the DA and VE processes in HNCO is exactly of this nature. The Wigner cusps and threshold peaks are prominent features in the observed cross sections [1,2]. It is known that the proper description of these phenomena involves the energy dependence of the effective potential, which is also inherently nonlocal [19,20]. In our

*Martin.Cizek@mff.cuni.cz

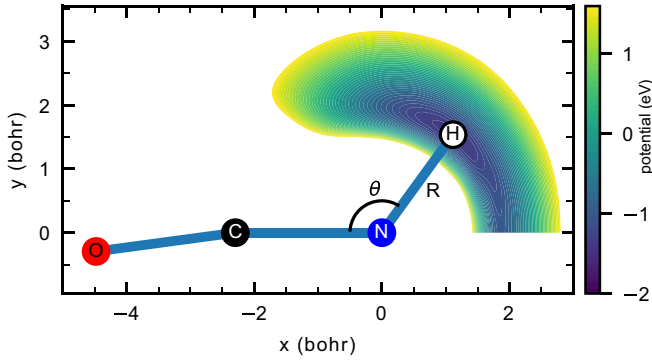


FIG. 1. Illustrative picture of the equilibrium molecular geometry and the neutral potential dependence on the hydrogen-atom position.

previous work, we built on the pioneering work of Domcke, Cederbaum, and collaborators [21,22] and developed a computationally tractable *ab initio* approach to treat such phenomena in diatomic molecules [23–27]. We also used the same approach to treat the one-dimensional stretching motion of the hydrogen atom in electron collisions with the HNCO molecule [1,2].

To our best knowledge, the only attempts to treat polyatomic nonlocal dynamics include a model proposed by Estrada *et al.* [28] and more recently Ambalampitiya and Fabrikant [29] derived a two-dimensional nonlocal model to calculate the internal energy of polyatomic fragments in DA. We have recently also treated the nonlocal dynamics of three vibronically coupled discrete states in the continuum and we have also included their vibronic coupling through the electronic continuum to describe the experiments for energy-loss spectra of electrons colliding with CO₂ molecules [30–32]. The treatment contained four vibrational degrees of freedom but was limited only to geometries close to the equilibrium geometry of the neutral molecule. The wave functions could therefore be expanded in the harmonic-oscillator basis. Here, for the HNCO molecule, the dissociation motion is crucial and we have to treat the dynamics in a much wider range of the dissociative coordinates. Since both construction of the model and the numerical treatment of the dynamics is time-consuming in the nonlocal framework, we decided to keep the position of the N, C, and O atoms fixed and treated just the motion of the hydrogen atom. We thus extended the one-dimensional model from Ref. [1,2] including the HNC bending angle as the dynamical degree of freedom. As compared with the model of Ambalampitiya and Fabrikant [29] where one coordinate was describing the internal excitation of the fragment, both coordinates participate in the dissociative motion in our case.

The paper is organized as follows: First, we discuss the theory in Sec. II. Section III is devoted to the construction of the model based on the fixed-nuclei electron-molecule scattering calculation using the *R*-matrix method. Finally, we discuss the calculated cross sections for various processes and their interpretation in Sec. IV. The conclusions are summarized in Sec. V. The technical details of the calculation and the description of the model parameters are deferred to Appendices A–C.

II. THEORY

The theoretical treatment described below follows the treatment of diatomic molecules [19,24]. Here we explain the necessary generalizations and notation.

We start by describing the vibrational motion in the target HNCO molecule. To simplify the model we neglect the slight deviation of the OCN bond angle from a straight line ($\angle\text{OCN} \simeq 175^\circ$ [33]), which makes the motion of the hydrogen atom axially symmetric. We parametrize its position q in spherical coordinates $q = (R, \theta, \varphi)$. The vibrational motion of the hydrogen atom in the neutral HNCO molecule is therefore described by the potential energy $V_0 = V_0(R, \theta)$ independent of angle φ . The motion of the hydrogen relative to the OCN radical conserves the angular-momentum projection to the OCN axis. In our calculation, we assume the molecule at sufficiently low temperature, i.e., this projection is assumed to be zero. All the nuclear wave functions are therefore also independent of the angle φ . The vibrational states $|\nu\rangle$ are found by solving the stationary Schrödinger equation

$$H_0|\nu\rangle = (T_N + V_0)|\nu\rangle = E_\nu|\nu\rangle, \quad (1)$$

where T_N is the kinetic-energy operator for the motion of the hydrogen nucleus, E_ν the energy of the vibrational state and the symbol ν stands for the collection of quantum numbers necessary to identify the vibrational state. This equation is solved in spherical coordinates by expanding the vibrational states into spherical harmonics (see Appendix A).

The theoretical description of the electron collision with the molecule is based on the projector operator formalism. The interaction of the electron with the molecule at fixed molecular geometry is described as an interaction of a discrete state $|\phi_d\rangle$ with the continuum $|\phi_\epsilon\rangle$ [19]. We follow closely the approach used in previous calculations [1,2] which treated the dynamics of hydrogen motion as one-dimensional motion in the radial direction R and generalize it to the present axially symmetric case.

The vibrational dynamics of the anion collision complex formed by the electron collision with the molecule is described by the projection $|\psi\rangle = \langle\phi_d|\Psi\rangle$ (scalar product over electronic degrees of freedom only) of the full wave function $|\Psi\rangle$ on the discrete state. This way we project out the electronic degrees of freedom and the function $|\psi\rangle$ is the solution of the equation

$$[E - T_N - V_d - F(E)]|\psi\rangle = V_{d\epsilon_i}|\nu_i\rangle, \quad (2)$$

where $V_d(q) = \langle\phi_d|H_{el}|\phi_d\rangle$ is the potential energy of the discrete state and $F(E)$ is called the nonlocal potential or the level-shift operator. It describes the modification of the potential energy $V_d(q)$ due to the presence of the electron continuum and it is a nonlocal operator in coordinate q depending on the collision energy E . Thanks to this dependence the dynamics is sensitive to the spectrum of the neutral molecule and the nonlocal approach can describe correctly the behavior of the dynamics close to the VE thresholds [34,35]. The quantity $V_{d\epsilon_i}(q) = \langle\phi_d|H_{el}|\phi_{\epsilon_i}\rangle$ is the coupling matrix element of the discrete state to the electron continuum. It describes the formation of the collision anion complex by attachment of the incident electron with the energy ϵ_i to the initial vibrational

state $|v_i\rangle$ with energy E_{v_i} . The discrete state-continuum coupling $V_{d\epsilon_i}(q) = \langle \phi_d | H_{el} | \phi_{\epsilon_i} \rangle$ also enters the expression for the nonlocal potential $F(E)$ (see Appendix C). To avoid enforcement of the outgoing boundary condition in Schrödinger equation (4) we solve the Lippmann-Schwinger equation

$$|\psi\rangle = |\phi_i\rangle + G_d(E)F(E)|\psi\rangle \quad (3)$$

instead. Here the vector $|\phi_i\rangle$ characterizes the initial state and for the $e^- + AB$ channel it has the form

$$|\phi_i\rangle = G_d(E)V_{d\epsilon_i}|v_i\rangle. \quad (4)$$

The outgoing boundary condition is taken into account automatically by taking the Green's operator $G_d(E)$

$$G_d(E) = (E - T_N - V_d + i\epsilon)^{-1} \quad (5)$$

in the retarded form which is ensured by imaginary positive infinitesimal $i\epsilon$ in the expression above. The details on the evaluation of the Green's operator $G_d(E)$ and the nonlocal potential $F(E)$ and also on the procedure for the solution of the equation (5) for $|\psi\rangle$ are given in Appendix C. The whole procedure is based on the expansion of the axially symmetric dynamics in the spherical harmonics and on solving the coupled integrodifferential equations for the wave function.

The T -matrix element relevant to the vibrational excitation into the final vibrational state $|v_f\rangle$ reads

$$T_{VE} = \langle v_f | V_{d\epsilon_f}^* | \psi \rangle \quad (6)$$

where ϵ_f is the energy of the outgoing electron determined from energy conservation during the collision

$$E = E_{v_i} + \epsilon_i = E_{v_f} + \epsilon_f.$$

The T -matrix element (8) is numerically evaluated from the scattering solution $|\psi\rangle$ expressed in spherical harmonics as explained in detail in Appendix C. Assuming energy normalization of scattering states, the differential cross section is given by

$$\frac{d\sigma_{VE}}{d\Omega} = \frac{(2\pi)^4}{k_i^2} |T_{VE}|^2, \quad (7)$$

where k_i is the momentum associated with the energy $\epsilon_i = \frac{1}{2}k_i^2$ of the incident electron. The integral cross section is obtained by integrating over electron-scattering angles and averaging over the orientation of the molecule, resulting in

$$\sigma_{VE} = \frac{4\pi^3}{k_i^2} |T_{VE}|^2. \quad (8)$$

The T matrix of the DA process can be extracted from the wave function in the asymptotic region as the wave function has the form of the outgoing spherical wave with amplitude given by the T matrix

$$\lim_{R \rightarrow \infty} \psi(R, \theta) = \frac{1}{R} T_{DA}(E, \theta) e^{iKR}, \quad (9)$$

where $K = \sqrt{2ME}$ is the momentum of the dissociative motion calculated from the energy conservation with the mass of dissociating hydrogen M . Elements of the T matrix contain dependence on the direction θ of the outgoing hydrogen. To

obtain the integral cross section we average over the orientation of the molecule and, assuming the partial wave expansion of ψ (see Appendix C), we get the expression for the DA integral cross section:

$$\sigma_{DA} = \frac{(2\pi)^2 K}{k_i^2 M} \lim_{R \rightarrow \infty} \sum_l |\psi_l(R)|^2. \quad (10)$$

III. MODEL

The equilibrium geometry of the HNCO molecule can be approximated by the axially symmetric model because the NCO part of the molecule is nearly linear. Our model is constructed by fixing the positions of N, C, and O atoms in an equilibrium geometry and moving the position $q = (R, \theta, \varphi)$ of the hydrogen atom in the molecular plane. The final model is obtained by assuming axial symmetry, i.e., all model parameters are independent of φ . We skip the φ dependence in the rest of this paragraph. The two remaining degrees of freedom $q = (R, \theta)$ have the meaning of the length R of the NH bond and HNC bending angle θ .

The nonlocal resonance model is fully described by three functions $V_0(q)$, $V_d(q)$, $V_{d\epsilon}(q)$. The potential surface of the neutral molecule $V_0(q)$ was obtained by fitting energies computed using the coupled-cluster approach CCSD-T [36,37] with the augmented correlation-consistent basis set aug-cc-pVTZ [38] as implemented in MOLPRO package of quantum chemistry programs [39]. Computed energies were fitted using two-dimensional splines. To obtain correct asymptotic behavior the spline was smoothly joined on the edge of the calculated area with a term proportional to R^{-6} .

The discrete-state potential-energy surface $V_d(q)$ and the coupling element $V_{d\epsilon}(q)$ were obtained by fitting eigenphase sums obtained from the R -matrix scattering calculations. We performed fixed-nuclei R -matrix calculations using the UK molecular R -matrix suite of codes [40]. We employed the static-exchange plus polarization model [41] in which the target molecule is described on the Hartree-Fock level using the cc-pVDZ basis. Eigenphase sums were calculated for the geometries spanning $\theta = 70^\circ - 180^\circ$ and $R = 1.3 - 3.0$ a.u. The resulting eigenphase sums were parametrized by the generalized Breit-Wigner formula

$$\delta(q, \epsilon) = \delta_{BG}(q, \epsilon) + \tan^{-1} \frac{\Gamma(q, \epsilon)/2}{\epsilon - V_d(q) - \Delta(q, \epsilon)}, \quad (11)$$

with

$$\Gamma(q, \epsilon) = 2\pi |V_{d\epsilon}(q)|^2, \quad (12)$$

$$\Delta(q, \epsilon) = \text{P} \int \frac{|V_{d\eta}(q)|^2}{\epsilon - \eta} d\eta, \quad (13)$$

where P denotes the Cauchy principal value of the integral.

The details on the functional form of the model parameters and the coefficients obtained by the fitting procedure are summarized in Appendix B. Here we give just some general remarks. The discrete state potential $V_d(q)$ is composed of two parts. The short-range part is expanded in the spherical harmonics $Y_{lm}(\theta)$ with $m = 0$ and the expansion coefficients exponentially decreasing with the radial distance R . The long-range part has a polarization form R^{-4} for $R \rightarrow \infty$. Similarly

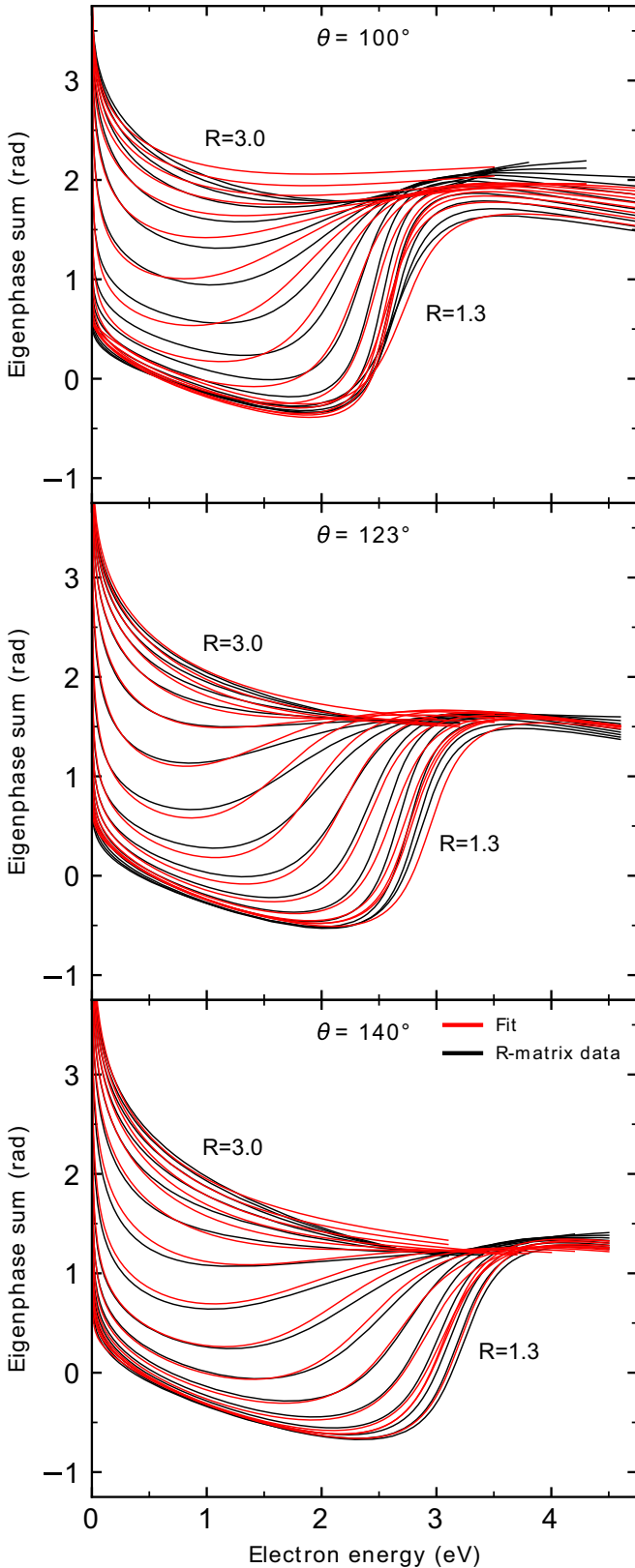


FIG. 2. Calculated R -matrix eigenphase sums and corresponding fits for three selected angles and $R = 1.3$ – 3.0 bohr.

the discrete-state-continuum coupling $V_{d\epsilon}(q)$ is expanded in spherical harmonics to capture the dependence on the angle θ and the expansion coefficients have a similar form as in the

previous 1D model [1] separable in R and ϵ to facilitate the analytic calculation of the integral Hilbert transform formula for $\Delta(q, \epsilon)$. The background phase shift $\delta_{BG}(q, \epsilon)$ is fitted as a smooth function with as few parameters as possible capturing the threshold behavior $\epsilon \rightarrow 0$.

The resulting fit compared with the eigenphase sums obtained by the R -matrix calculations is shown in Fig. 2. The quality of the fit in the equilibrium geometry is comparable with the previously used one-dimensional model [1]. The quality for the higher values of the angle is similar to the equilibrium geometry but gets progressively worse for smaller angles. Since the wave function in the dynamics does not probe this region significantly we do not consider it as a major flaw of the model. The data show the narrow resonance at 2.5–3.0 eV that gets broader and shifts towards lower energies until it disappears in the threshold behavior. This behavior, known from a previous study [1], is not much altered by changing the angle θ . The fit could be improved by adding more terms in the analytic form of the model functions defined in Appendix B. We decided not to increase the complexity of the model further and to keep it relatively simple, since the improvement of the fit would not make a significant step toward a more realistic model considering the other approximations inherent to the R -matrix approach generating the scattering data and the approximations in the subsequent treatment of the dynamics.

Figure 3 shows the potential surfaces obtained by the fitting procedure for three selected geometries. Note that the local complex potential approximation $V_{loc}(q) - \frac{i}{2}\Gamma(q)$ shown in the figure is defined as the position of the K -matrix pole and the imaginary part of $F(E)$ at this energy [27]. The energy and the width of the resonance increase for higher angles (approaching linear geometry). Otherwise, the potentials are qualitatively similar to the equilibrium angle. This is a strong indication that the dynamics is essentially one-dimensional and the stretching will be weak as we already noted in Ref. [1]. On the other hand, the present model will enable us to test the quality of the 1D approximation and predict the motion in the bending direction and its coupling with the stretching and dissociation of the anion.

IV. RESULTS

Before discussing the scattering calculations and the cross sections we first look at the vibrational states of the target neutral HNC molecule.

A. Final vibrational states of the neutral molecule

We use the *ab initio* calculated potential-energy surface $V_0(R, \theta)$ to find the vibrational states from Eq. (3) solved in spherical coordinates by expansion of the states $|\nu\rangle$ in spherical harmonics. The resulting wave functions of the lowest 32 states are shown in Fig. 4. The potential is, in principle, anharmonic, but as we see from Fig. 1 its shape is approximately separable in spherical coordinates. This is reflected in the character of the wave functions, the majority of which can be classified with number n_b of excitations in bending mode and number n_s of stretch excitations. The leading feature is the nodal structure of the wave functions. The number of

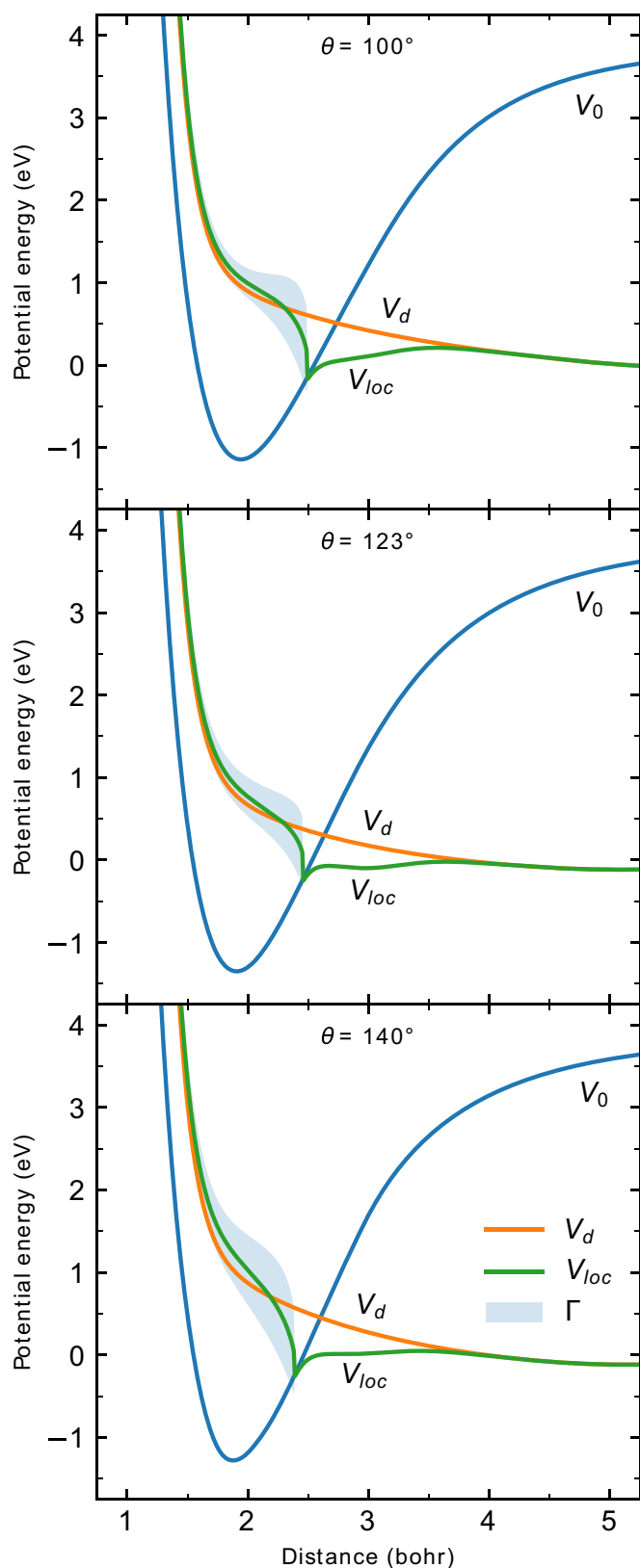


FIG. 3. Potential-energy surfaces of the model for three selected angles. Shaded area shows the width of the resonance.

horizontal nodal lines thus determines the number of bending excitations n_b and the number of vertical lines corresponds to number of excitations n_s of the stretching mode. We show

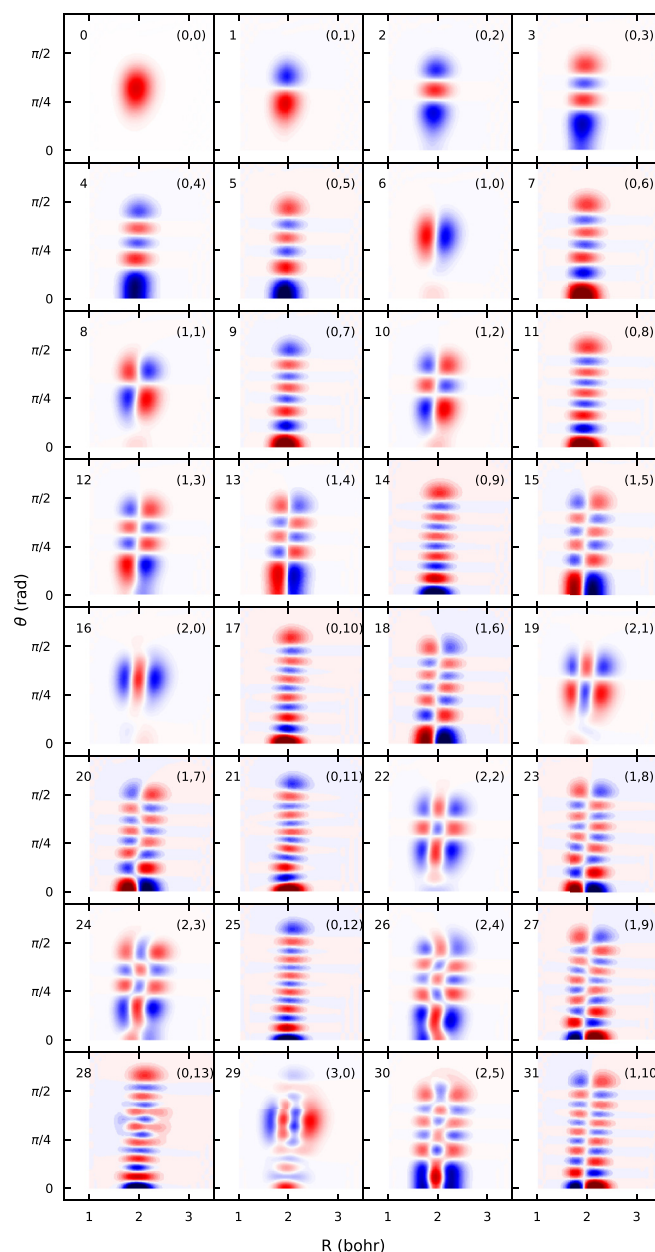


FIG. 4. Wave functions of vibrational states of the neutral molecule. Numbers in the top-left corner show numbering of the state with respect to increasing energy; pairs in brackets in the top right corner denote the number of stretching and bending excitations.

this classification of the states in Fig. 4 by printing (n_s, n_b) in the top-right corner. The number in the top-left corner gives the ordinal number for each state with respect to increasing energy E_v . The figure contains several states where the classification by (n_s, n_b) starts to break. This happens when energy of two or more states is close enough that they become mixed. Weak signatures of the mixed character can be seen, for example, in states number 6 and 7, where a maximum close to $\theta = 0$ is observed in state number 6. The vertical nodal plane does not reach this maximum and the nodal planes of the state 7 are not completely horizontal. The mixing becomes even more apparent at higher energies. For example, the states 28 and 29 are rather strongly mixed, but still their character

is predominantly $(n_s, n_b) = (0, 13)$ and $(3, 0)$, respectively. In the rest of the section we use the quantum numbers n_b and n_s determined from Fig. 4 to classify the states.

B. Details of the numerical calculation

We start our discussion by giving the details of the numerical procedure used to calculate the cross sections. We have calculated the cross section of the using theoretical framework from Sec. II and the model of HNCO molecule described in Sec. III with the details given in Appendixes. Note that the spherical harmonics used in the expansions effectively reduce to the corresponding Legendre polynomials due to the axial symmetry and are real. The Lippmann-Schwinger equation (5) was solved using Schwinger-Lanczos algorithm [42]. The calculations were performed using 18 partial waves ($l = 0, 1, \dots, 17$ with axial symmetry $m = 0$) for the expansion of the wave function and radial grid of approximately 1000 points spanning from $1a_0$ to $15a_0$. Values of the parameters were chosen to ensure that errors of T -matrix elements are below 1% across the investigated range of energies with respect to the change of these parameters. Errors of elements for higher excited vibrational states rise as the number of partial waves needed for a good description of the states also rises. For the expansion of the nonlocal potential, we used states up to the energy of 7 eV, i.e., approximately 1800 states. In general, the number of states needed for a good description of the nonlocal potential is the main overall factor for the time cost of the calculation because it grows exponentially with the number of included degrees of freedom.

The convergence of the Schwinger-Lanczos algorithm depends heavily on the total energy of the system. The number of iterations needed to converge in double precision is 15–25 for energies well below the threshold energy for DA. Near the threshold energy (1.1 eV), the number of iterations rises up to approximately 200 and then it decreases again to around 50 further away from the threshold.

C. Dissociative attachment cross section

The original 1D model of the dissociative electron attachment to the HNCO molecule [1] was rather successful in the interpretation of the observed cross section. To see the effect of the additional nuclear degree of freedom on the DA cross section, we used the two-dimensional (2D) model with the angular coordinate restricted to the equilibrium value $\theta = 123^\circ$ to construct a 1D model and solved the dynamics with the same procedure that was used in Ref. [1].

Figure 5 shows the DA cross section calculated with both one- and two-dimensional models. We observe that the main features of the cross-section curves remain the same. A high threshold peak is followed by Wigner cusps at energies corresponding to the channel opening of stretch excitations $(n_s, 0)$. The energy positions of the cusps are shifted because the vibrational energies differ between the 1D and 2D models. The 2D-model cross section is comparable to the one obtained within the 1D model, yet larger by 0%–50%. In the results for the 2D model, the bending motion is manifested in the appearance of additional smaller cusps at energies approximately 0.1 eV higher than the dominant Wigner cusps due to

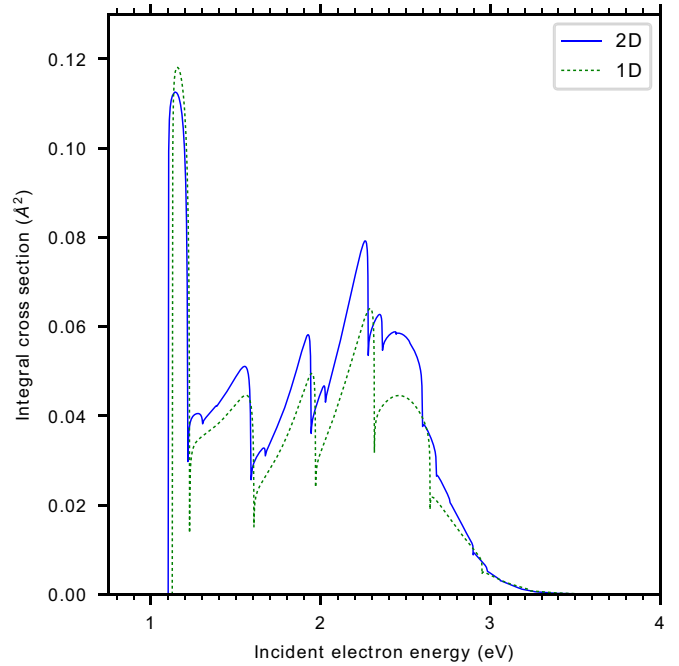


FIG. 5. Integral cross section for dissociative attachment. Comparison of the full 2D calculation with 1D model restricted to NH-stretching motion.

the opening of the higher stretch excitation channels. These cusps are caused by channel opening of the first bending excitations $(n_s, 1)$. The magnitude of the additional cusps due to the excitation of even higher bending channels is very small and these cusps are barely distinguishable in the figure.

Additional information available from the 2D calculation is the angular distribution of DA products in the molecular frame. The distribution is obtained from the values of the wave function (11) in the asymptotic region. In our case, the outgoing wave is centered in a peak of the width of 40° around the equilibrium angle $\theta = 123^\circ$. This remains true for the entire range of investigated energies and reflects the spreading of the vibrational ground state. This feature is another illustration of the dominantly radial character of the dissociative motion.

Agreement with experimental results is similar to the previously published 1D model. The magnitude of the cross section and relative height of the threshold peak is sensitive to the choice of certain parameters of the model and could be fine tuned to better reproduce the experimental data, but this procedure does not provide any additional insight. More interesting would be the inclusion of additional degrees of freedom, but this goes beyond the scope of current work.

D. Vibrational excitation—comparison with experiment

We have already studied the vibrational excitation of the stretch vibration and its first overtone in Ref. [2]. Similarly, for the dissociative detachment, the results were in good agreement with the experiments. Here we compare the new 2D calculation with the 1D restricted model in Fig. 6 (top) for excitation to state $(1, 0)$ (one quantum of stretching vibration). The shapes of the two curves are very similar. A notable

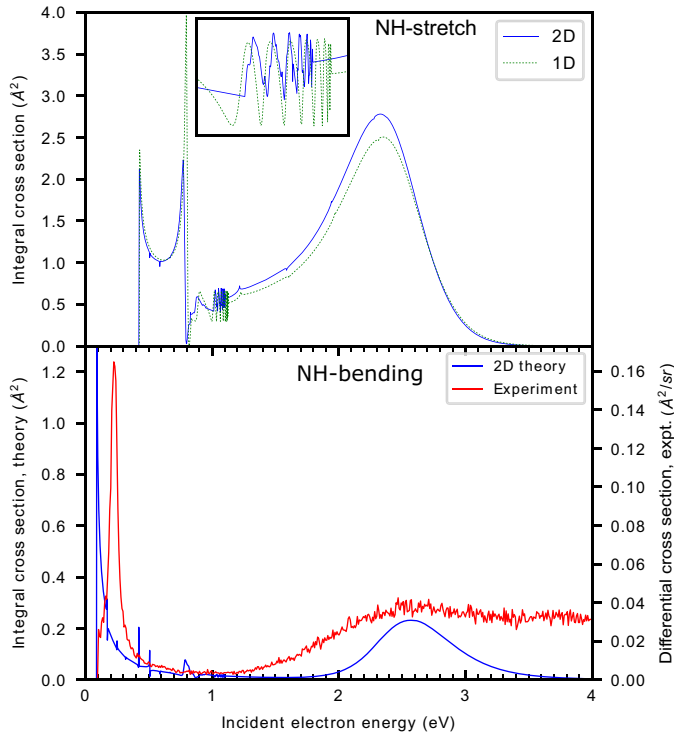


FIG. 6. Integral cross section for excitation of the stretch vibration (top) and bending vibration (bottom). We compare 1D versus 2D calculation for stretching and 2D calculation versus experimental cross sections of Ref. [2]. The detail of the boomerang oscillations is shown in the inset.

difference is in the magnitude of the second peak corresponding to the opening of $(2,0)$ channel which is reduced by almost 50%, which makes the results closer to experimental data in Ref. [2]. The cross section of the 2D model is about 10% higher for energies above the DA threshold. The 1D model also exhibits boomerang oscillations near the threshold of DA similar to Ref. [43]. We were curious if these oscillations survive the inclusion of the second degree of freedom. Indeed they are also present in the 2D model but with reduced magnitude and the emergence of smaller secondary oscillations (see the inset in Fig. 6). The explanation of this effect remains similar to the 1D case and is easier to describe in the time-dependent picture. Given a sufficiently shallow potential, the wave packet with energy near the threshold can travel a long distance to the turning point where it is reflected back. The electron detachment from the reflected wave then interferes with the direct detachment in the central region. This interference causes oscillatory behavior in the cross section. With the addition of angular motion, the shape of the 2D potential surface allows the wave packet to spread also in the angular direction. This creates secondary smaller oscillations in the cross section. This mechanism can be seen from the anion wave functions shown in Fig. 8 which we discuss in detail below.

The previously unavailable result, the excitation cross-section curve of the bending mode $(0,1)$, is shown in Fig. 6 (bottom). It exhibits a high and narrow threshold peak and broader resonance centered around 2.6 eV. The position of the resonance is shifted by 0.2 eV towards higher energies

(relative to the peak in the stretch vibration). This is consistent with the experimental cross section (measured in Ref. [2]) which shows a similar shift. Above the resonance, the theoretical cross section quickly decreases while experimental results show different behavior. This is caused by a presence of A'' resonance around 4 eV (as discussed in Ref. [2]) which is not included in our model. There are a number of smaller cusps and peaks caused by the opening of higher vibrational channels in the theoretical curve. These are too narrow to be resolved in the experiment. There is also a broader peak around 0.8 eV, its origin is discussed further below. The peak, which is present in the theoretical curve just at the threshold, is shifted by approximately 0.1 eV to higher energies in the experiment. The origin of this shift is unknown. We can only speculate that this may be an effect of the other vibrational degrees of freedom that are not present in the model. Indeed the frequency of the bending vibrations is low and close to the other modes. The reduced dimensionality of our model can also be responsible for the narrowing of the main resonance peak at 2.6 eV with respect to the experiment. Apart from these two differences, the theoretical curve is in qualitative agreement with the experiment. Considering the comparison with the experimental cross sections, we also have to keep in mind that the experiment measures the differential cross section at the scattering angle of 135° while we calculated the integral cross section. We usually did the same type of comparison also in the case of diatomic molecules [24,34]. We do not expect a big difference in the shape of the cross-section curves, since the resonance is dominated by the s -wave contribution. Although higher partial waves may contribute to some distortion of the cross-section curves, we do not expect modification of the sharp structures.

Figure 7 shows higher excitation cross sections for selected vibrational modes sorted into three categories, overtones of pure bending excitation $(0, n_b)$ and combined excitations $(1, n_b)$ and $(2, n_b)$ as compared with the elastic cross section. There are several interesting common features observed in all excitation curves. The cross-section curves have many peaks in the region below threshold energy for the dissociative attachment and a broad resonance between 2 and 3 eV. The cross sections also exhibit changes of up to two orders of magnitude in the region starting at 0.7 eV. Most of the peaks originate from the opening of higher vibrational channels because they are positioned at their corresponding energies. The boomerang oscillations are suppressed in this plot because of the logarithmic scale used to fit all curves in one plot. We also see that the stretching vibration is much more efficient than bending, consistently with the essentially radial picture of the dynamics.

E. Wave functions and interpretation of the structures

To get a deeper insight into the dynamics and origin of the structures in the cross sections we plot in Fig. 8 (left) the wave function projected on discrete electronic state, i.e., the quantity $\psi(R, \theta)$ obtained by solving (5). This wave function reflects the dynamics of the collision complex within the time-independent picture of the collision. Figure 8 (right) also shows elastic and vibrational excitation cross sections for the fundamental excitation $(0,1)$ and $(1,0)$ with six energies

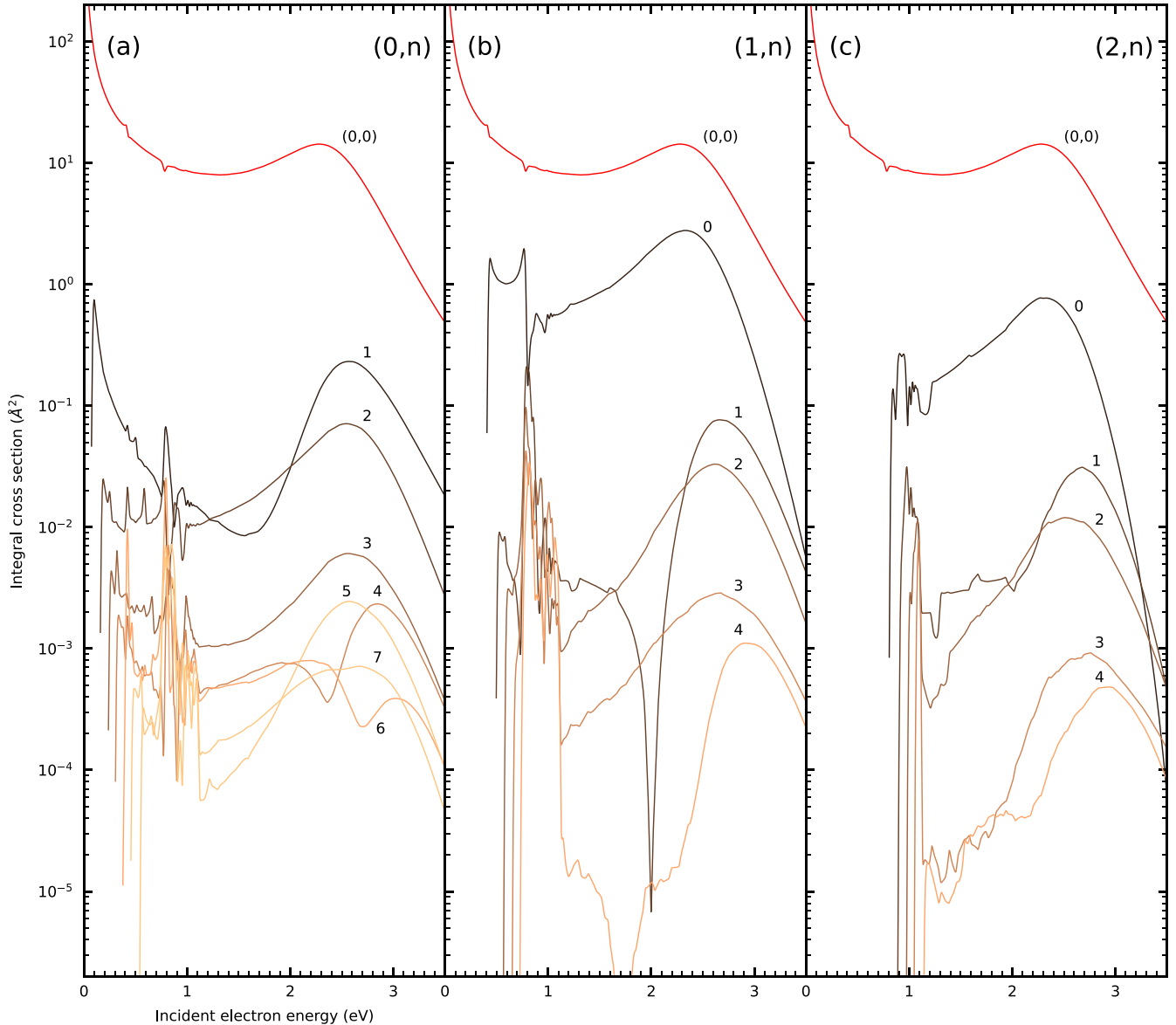


FIG. 7. Overview of excitation curves. Panel (a) shows pure bending excitations $(0, n)$, (b) shows single stretching excitations $(1, n)$, and (c) shows double stretching excitation $(2, n)$. Each curve is labeled by its respective number of bending excitations n .

marked by dashed vertical lines. These are the energies for which the wave function in the left panel is calculated.

In the case of $(1,0)$ excitation, the effect of the channel opening is evident from anion wave functions shown in Fig. 8. The wave function closely reproduces the $(1,0)$ vibrational state of the neutral molecule [note that the wave function is over-saturated in the Fig. 8(b) due to too large magnitude resulting from the vibrational Feshbach resonance].

The same effect cannot be easily seen for bending channel openings because the magnitude of change is several orders of magnitude smaller. The wave function in Figs. 8(e) and 8(f) is calculated for the energies in the region of the boomerang oscillations. We can see the interference of the outgoing and back-reflected waves in the vertical nodal structure but also undulations in the bending direction.

The overall shape of the wave functions confirms that the dynamics is mostly happening close to the equilibrium angle

$\theta = 123^\circ$. This is violated in the region of boomerang oscillations as seen in the last two wave functions. The amplitude close to angle $\theta = 0$ (corresponding to the value π on the y axis) is larger than one may expect because it corresponds to the hydrogen atom close to the carbon and the oxygen. This is an artifact of our model since we extrapolated the potential V_d in this region from the scattering data in the angular range $\theta = 90^\circ - 180^\circ$ which underestimated the potential in this region. This feature of our model should not influence the conclusions drawn from our calculations except for the details of the shape of the cross sections in the boomerang oscillation region.

F. Two-dimensional electron energy-loss spectrum

Finally, Fig. 9 shows cross-section curves as the two-dimensional electron energy-loss spectrum, i.e., the cross

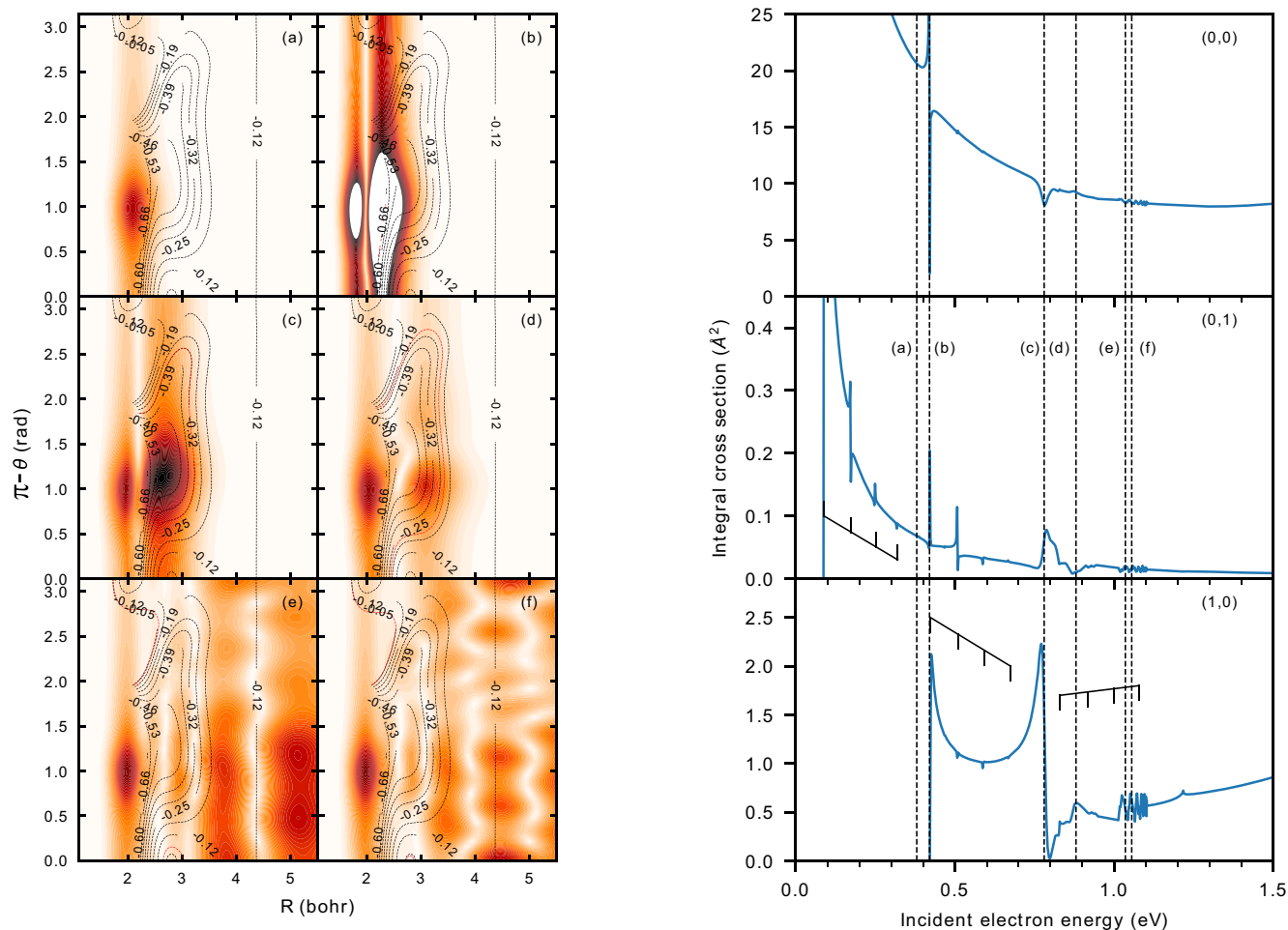


FIG. 8. Absolute value of wave functions (left) at energies marked as vertical lines in the cross sections (right). The figure on the right also shows the positions of the opening of individual vibrational excitation channels that are relevant for structures appearing in the cross sections.

section marked in color scale is plotted as a function of the incident electron energy (vertical axis) and the electron energy loss (horizontal axis). The picture is dominated by vertical lines, marking the positions of the individual electron energy losses associated with the respective final states of the neutral molecule. The excitation of pure stretching vibration and its overtones ($n_s, 0$) dominate the spectrum. The individual electron energy-loss lines exhibit a maximum near the resonance electron energy $E_i \simeq 2.5$ eV. The cross section is also enhanced near the threshold line, as expected for the molecule with a strong dipole moment. In addition to this expected behavior, we see a progression of structures for incident energies $E_i \simeq 0.6$ – 1.1 eV. From the previous discussion, we see that this behavior is related to the expanded freedom of motion of the anion close to the crossing with the potential-energy surface of the neutral molecule and is associated with the appearance of the boomerang oscillations. This behavior is also limited from above by the dissociative attachment threshold.

V. CONCLUSIONS

The main achievement of the presented work is the generalization of our nonlocal discrete-state-in-continuum approach, which we used previously in diatomic molecules, to include

two degrees of freedom that can both participate in dissociative attachment. We developed new numerical methods to treat the dynamics by expanding the angular degrees of freedom in spherical harmonics and by calculating the Green's function in the dissociative attachment channel on the grid by numerically solving the coupled-channel Schrödinger equation. The final nonlocal dynamics is treated by the Schwinger-Lanczos iteration scheme. The current work can be viewed as complementary to our recent work [30–32] where we also included more degrees of freedom in the nonlocal calculation, but the dynamics was limited in space, allowing thus only treatment of vibrational excitation. The currently developed approach can be used for future calculations of other polyatomic molecules of interest in the description of various processes of both technological and fundamental processes that require inclusion of the dissociative attachment channel (see, for example, Refs. [7,44]).

We also constructed a two-dimensional model for the dynamics of the HNCO^- collision complex created in $e^- + \text{HNCO}$ collision. The model parameters were extracted from *ab initio* data for fixed-nuclei electron-molecule calculation obtained with the *R*-matrix approach. We also applied the methods developed here for the treatment of the dynamics of this system. The results show that the inclusion of the bending

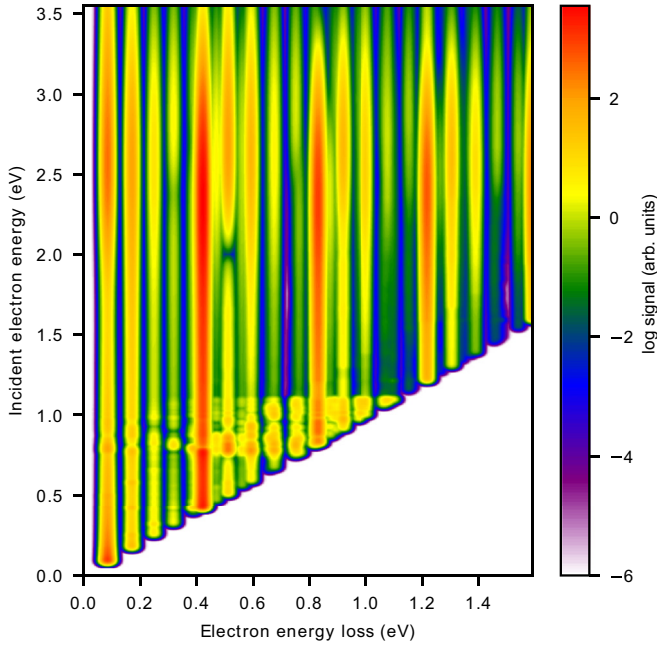


FIG. 9. Two-dimensional electron energy-loss spectrum. The color codes the cross section in the logarithmic scale. The discrete energy loss spectrum is broadened by assuming a Gaussian profile of 30meV FWHM in the horizontal direction. No broadening in the incident energy (vertical direction) is applied to enhance the structure due to the channel coupling and boomerang oscillations.

motion of the hydrogen atom does not significantly change the outcome of the calculation for previously treated cross sections of dissociative attachment and vibrational excitation of the NH stretching motion. The uncertainty due to the choice of parametrization made during the fitting procedure introduces bigger error in the calculation than the restriction to 1D. This validates previously published calculations treating the collision using a 1D model and confirms that the dynamics is essentially radial in the NH direction.

On the other hand, the current generalization of the model allows for studying the coupling of the stretching and bending vibration motion. We also show that the boomerang oscillations are not completely destroyed by the inclusion of the bending motion. The 2D electron energy-loss spectrum was also calculated for the model.

ACKNOWLEDGMENTS

This work was supported by the Czech Science Foundation Project No. 19-20524S (M.Č., K.H.) and by the Charles University Grant Agency Project GAUK No. 552419 (J.T.).

APPENDIX A: CALCULATIONS OF THE VIBRATIONAL STATES OF THE NEUTRAL MOLECULE

To find the vibrational states of the neutral molecule, we have to solve Eq. (3). First, we expand the potential energy of the neutral molecule in spherical harmonics:

$$V_{JJ'}^0(R) = \int Y_J(\theta)^* V_0(R, \theta) Y_{J'}(\theta) d\Omega, \quad (\text{A1})$$

where $J = (l, m)$ and $d\Omega$ means integration over the unit sphere. Note that, since the potential V_0 is axially symmetric with respect to the z axis, we need only the spherical harmonics with $J = (l, m = 0)$, i.e.,

$$Y_l(\theta) = \sqrt{\frac{2l+1}{2\pi}} P_l(\cos \theta).$$

We now substitute the expansion of the vibrational wave function

$$|v\rangle = \sum_l \frac{1}{R} \chi_{vl}(R) Y_l(\theta) \quad (\text{A2})$$

into Eq. (3) to get the coupled set of equations

$$\begin{aligned} \frac{1}{2M} \left(-\frac{d^2}{dR^2} + \frac{l(l+1)}{R^2} \right) \chi_{vl}(R) \\ + \sum_{l'=0}^N V_{ll'}^0 \chi_{vl'}(R) = E_v \chi_{vl}(R), \end{aligned} \quad (\text{A3})$$

where we introduced the cutoff N for the expansion into the spherical functions. We represent this set in the Fourier basis in the box $R \in (0, R_{\max})$, where R_{\max} is the cutoff radius and find the eigenenergies E_v and eigenvectors in the matrix representation. We ensured that both N and R_{\max} are sufficiently large to achieve convergence.

APPENDIX B: PARAMETERS OF THE MODEL

In this Appendix (and Table I), we describe the details of the parametrization of the model functions $V_d(R, \theta)$, $V_{d\epsilon}(R, \theta)$, and $\delta_{BG}(R, \theta, \epsilon)$. The angular dependence of these terms is expanded in spherical harmonics. Since our model is axially symmetric we only use functions with $m = 0$. The energy dependence of the background phase shifts is given by the low-energy behavior for molecules with the supercritical dipole

$$V_{d\epsilon}(R, \theta) = \sum_n f_n(\epsilon) g_n(R, \theta) = \sum_{n,l} f_n(\epsilon) g_{nl}(R) Y_{l0}(\theta). \quad (\text{B1})$$

Two energy terms $f_n(\epsilon)$ were used in the expansion

$$\begin{aligned} f_1(\epsilon) &= e^{-\beta\epsilon}, \\ f_2(\epsilon) &= \sqrt{\epsilon} e^{-\beta\epsilon}. \end{aligned}$$

We set $\beta = 0.074 \text{ eV}^{-1}$. Our numerical experiments with the model indicate that the DA cross section is sensitive to value of β . The chosen value is obtained from fitting the model in the equilibrium geometry. The spatial part was described by functions

$$\begin{aligned} g_{1l}(R) &= g_{11l} e^{-g_{12l}(R-g_{13l})^2}, \\ g_{2l}(R) &= g_{1l}(R) [g_{21l} - g_{22l} e^{-g_{23l}(R-g_{24l})}]. \end{aligned}$$

The anion potential surface has the form

$$\begin{aligned} V_d(R, \theta) &= \sum_l v_l(R) Y_{l0}(\theta) \\ &+ \frac{\alpha}{(R-3)^4 + (R-3)^2 + 408.2}, \end{aligned}$$

TABLE I. The values of model parameters used for the calculations. All values are in atomic units.

$l =$	0	1	2	3	4
v_{1l}	227.9	18.39	18.35	18.39	18.4
v_{2l}	2.714	4.415	3	2.806	2.646
v_{3l}	0.02765	-0.03433	-0.05135	0.01049	-0.1082
v_{4l}	1.024	1.256	2.46	1.068	1.652
g_{11l}	0.1124	0.05198	-0.01995	0.03797	-0.1181
g_{12l}	-0.0108	1.206	0.07052	0.5527	1.63
g_{13l}	1.814	1.55	0.7734	0.2933	0.4837
g_{21l}	14.87	-7.779	6.183	7.89	-1.82
g_{22l}	16.26	20.28	-0.7494	-0.2993	15.91
g_{23l}	1.654	1.645	0.6362	1.203	0.873
g_{24l}	1.92	0.3619	-0.2197	0.2445	-1.553
a_{1l}	2.259	0.201	0.2004	-0.2364	-0.05685
a_{2l}	-0.9516	-0.0154	-0.1294	0.1032	0.04811
b_{1l}	-0.0901	-0.0121	0.05554	-0.1631	-0.02803
b_{2l}	0.03377	-0.00968	-0.03879	0.08382	0.01215
c_{1l}	-0.2406	-0.8114	0.06296	-0.01097	-0.00642
c_{2l}	0.07504	0.2472	-0.01836	0.004487	0.002301

where

$$v_l(R) = v_{1l}e^{-v_{2l}R} + v_{3l}e^{-v_{4l}R},$$

and the asymptotic behavior is given by the term proportional to R^{-4} , where $\alpha = 2.25$ is the polarizability of the hydrogen atom.

We have also included the asymptotic shift of the V_d to obtain the correct threshold energy and threshold peak. The input data for the construction of the model do not take into account the change of equilibrium geometry of fragment NCO as the hydrogen atom leaves the molecule. This relaxation of the geometry decreases the threshold energy. To include the relaxation into the model we include an additional term for V_d :

$$\tilde{V}_d = V_d - \frac{\Delta E}{1 + e^{-3(R-3)}},$$

where $\Delta E = 0.25$ eV. The value of 0.25 eV gives lower threshold energy (difference of 0.1 eV) but qualitatively better threshold behavior of the DA cross section. The impact of this change was previously investigated for the 1D model in Ref. [1]. As a result of this change, the amplitude of the cross section is higher by approximately 20% but the shape of the cross-section curve remains unchanged.

The background eigenphase term was parametrized as

$$\delta_{BG}(R, \theta, \epsilon) = \sum_l \delta_l(R, \epsilon) Y_{l0}(\theta).$$

The energy dependence of the background phase shifts δ_l is chosen to be consistent with the low-energy behavior of scattering on molecules with the supercritical dipole moment. We assume a linear dependence on the radial coordinate:

$$\delta_l(R, \epsilon) = a_{1l} + a_{2l}R + (b_{1l} + b_{2l}R)\sqrt{\epsilon} + (c_{1l} + c_{2l}R)\ln\epsilon.$$

For our final model, spherical harmonics up to $l = 5$ were used. We restricted the geometries used for the fitting procedure in the range $\theta = 90^\circ - 160^\circ$ (centered around the

equilibrium angle of 123°). We also modified the term in electron-molecule coupling g_{1l}

$$\tilde{g}_{1l}(R) = \frac{g_{1l}(R)}{1 + e^{-2(R-3.1)}}. \quad (\text{B2})$$

As the fitting procedure is limited only to radial distances up to 3 a.u., this modification is needed to ensure that the coupling decreases sufficiently fast with radial distance.

APPENDIX C: NONLOCAL DISSOCIATIVE ATTACHMENT DYNAMICS IN TWO DIMENSIONS

In this Appendix, we explain the numerical procedure to solve the central equation of the nonlocal formalism

$$|\psi\rangle = |\phi_i\rangle + G_d(E)F(E)|\psi\rangle, \quad (\text{C1})$$

with

$$|\phi_i\rangle = G_d(E)V_{d\epsilon_i}|v_i\rangle, \quad (\text{C2})$$

where ϵ_i is the energy of the incident electron and $|v_i\rangle$ is the initial vibrational state of the molecule (we assume that this is the ground vibrational state). Nonlocal operator $G_d(E)$ is the Green's operator defined as

$$G_d(E) = (E - T_N - V_d + i\epsilon)^{-1}, \quad (\text{C3})$$

and $F(E)$ is the nonlocal potential defined as

$$F(E) = \int d\epsilon V_{d\epsilon}(q)G_0(E - \epsilon, q, q')V_{d\epsilon}(q'). \quad (\text{C4})$$

The energy E is the total energy of the system $E = \epsilon_i + E_{v_i}$. Since the resonance is predominantly of the s -wave character we assume that the discrete-state-continuum coupling is independent of the direction from which the incident electron comes

$$V_{d\epsilon}(q) = \frac{1}{\sqrt{4\pi}}V_{d\epsilon}(R, \theta), \quad (\text{C5})$$

and the electron does not bring any angular momentum.

Using the expansion of the neutral vibrational states (A2) and expanding also the wave function $|\psi\rangle$,

$$\psi(R, \theta) = \sum_l \frac{1}{R} \psi_l(R) Y_l(\theta), \quad (\text{C6})$$

in the spherical harmonics, we transform the main equation (C1) in the form

$$\begin{aligned} \psi_l(R) = & \sum_{l_1 l_2} \int dR' G_{dl_1}(E, R, R') \\ & \times \left\{ W_{l_1 l_2}(R') \chi_{v_l_2}(R') \right. \\ & \left. + \int dR'' F_{l_1 l_2}(E, R', R'') \psi_{l_2}(R'') \right\}, \quad (\text{C7}) \end{aligned}$$

where we introduced the spherical harmonic expansion of the discrete-state-continuum coupling element (B1),

$$W_{ll'}(R) = \sum_n W_{ll'}^{(n)}(R) f_n(\epsilon_i), \quad (\text{C8})$$

$$W_{ll'}^{(n)}(R) = \int Y_l(\theta) g_n(R, \theta) Y_{l'}(\theta) d\Omega, \quad (\text{C9})$$

and we also expanded the Green's operator $G_d(E)$ and nonlocal potential $F(E)$ in the spherical harmonics,

$$G_d(E) = \sum_{l_1 l_2} Y_{l_1}(\theta) \frac{1}{R} G_{dl_1 l_2}(E, R, R') \frac{1}{R'} Y_{l_2}(\theta'), \quad (\text{C10})$$

$$F(E) = \sum_{l_1 l_2} Y_{l_1}(\theta) \frac{1}{R} F_{l_1 l_2}(E, R, R') \frac{1}{R'} Y_{l_2}(\theta'). \quad (\text{C11})$$

The equation (C7) is solved for $\psi_l(R)$ on the grid using the Schwinger-Lanzos iteration algorithm [42] which is equivalent to resummation of (in general divergent) Born series [45]. The generalization of the algorithm for the present case is straightforward and we can use basically the same method as for diatomic molecules. What remains is to derive formulae to evaluate the expansion coefficients $F_{l_1 l_2}$ for the nonlocal potential and $G_{dl_1 l_2}$ for the Green's function in the local potential V_d .

1. Evaluation of nonlocal potential $F(E)$

To proceed with the evaluation of the nonlocal potential expansion $F_{l_1 l_2}$ we must project the definition (C4) on spherical harmonics. In doing this we use the expansion coefficients of the discrete-state-continuum coupling $W_{l_1 l_2}^{(n)}$ introduced above in formula (B1)

$$V_{d\epsilon} = \sum_n \sum_{l_1 l_2} Y_{l_1}(\theta) W_{l_1 l_2}^{(n)}(R) f_n(\epsilon) Y_{l_2}(\theta'), \quad (\text{C12})$$

and we also expand the Green's function $G_0(E)$ into bound states of the neutral molecule

$$G_0(E) = \sum_v \frac{|v\rangle\langle v|}{E - E_v + i\epsilon} \quad (\text{C13})$$

$$= \sum_{v l_1 l_2} Y_{l_1}(\theta) \frac{1}{R} \frac{\chi_{v l_1}(R) \chi_{v l_2}(R')}{E - E_v} \frac{1}{R'} Y_{l_2}(\theta'). \quad (\text{C14})$$

When these expansions are substituted into the definition (C4) we also have to perform the integral transformation

$$F_{mn}(E) = \int d\epsilon \frac{f_m(E) f_n(E)}{E - \epsilon + i\epsilon}. \quad (\text{C15})$$

This has the same form as the integrals which we used already for the 1D model in Ref. [1,2] and can be expressed in terms of the incomplete gamma function [46]. We therefore assume that the functions $F_{mn}(E)$ are known. We have now all the ingredient to conclude that

$$\begin{aligned} F_{ll'}(E, R, R') = & \sum_v \sum_{mn} \sum_{l_1 l_2} W_{ll_1}^{(m)}(R) \chi_{v l_1}(R) F_{mn} \\ & \times (E - E_v) \chi_{v l_2}(R) W_{l_2 l'}^{(n)}(R). \quad (\text{C16}) \end{aligned}$$

This expression can further be simplified by precalculating the sum

$$U_{vl}^{(n)}(R) = \sum_{l_1} W_{ll_1}^{(n)}(R) \chi_{v l_1}(R), \quad (\text{C17})$$

so that

$$F_{ll'}(E, R, R') = \sum_v \sum_{mn} U_{vl}^{(m)}(R) F_{mn}(E - E_v) U_{v l'}^{(n)}(R). \quad (\text{C18})$$

Similar expansions are then used to calculate T -matrix elements given by

$$T_{VE} = \langle v_f | V_{d\epsilon_f} | \psi \rangle. \quad (\text{C19})$$

Inserting the spherical harmonics expansion we obtain

$$\begin{aligned} T_{VE} = & \int dR \sum_n \sum_{ll'} \chi_{v_f l}(R) W_{ll'}^{(n)}(R) f_n(\epsilon_f) \psi_{l'}(R), \\ = & \int dR \sum_n \sum_l U_{v_f l}^{(n)}(R) f_n(\epsilon_f) \psi_l(R). \quad (\text{C20}) \end{aligned}$$

2. Evaluation of Green's function G_d

To obtain the partial-wave expansion of Green's function for general potential V_d we follow derivation from Ref. [47]. This approach expresses Green's function as a combination of sets of solutions of the underlying Schrödinger equation, one set being regular at origin and one regular at infinity. This is the generalization of the same problem from scattering in a spherically symmetric potential [48]. Using the spherical harmonic expansion of the general solution,

$$\phi(R, \theta) = \sum_J \frac{1}{R} \phi_J(R) Y_J(\theta), \quad (\text{C21})$$

we get the set of coupled equations

$$-\frac{d^2}{dR^2} \phi_l(R) + \sum_{l'=0}^N V_{ll'}^d \phi_{l'}(R) = K^2 \phi_l(R), \quad (\text{C22})$$

where we introduced potential matrix elements

$$V_{ll'}^d = 2M \int Y_{l'}(\theta) V_d(R, \theta) Y_l(\theta) d\theta + \frac{l(l+1)}{R^2} \delta_{ll'}. \quad (\text{C23})$$

By imposing regular boundary conditions at the origin $\phi_J(0) = 0$ we obtain a set of linearly independent solutions ϕ_{Jl}^R indexed by J with components l . Similarly imposing incoming boundary condition as $R \rightarrow \infty$ in the diagonal form $\phi_{Jl} = -ih_l^+(KR)\delta_{Jl}$ we obtain set of solutions ϕ_{Jl}^I . Then the expression for calculating Green's function elements can be written in matrix form:

$$\begin{aligned} g(R, R') &= \phi^R(R)(A^{-1})^T \phi^I(R')\Theta(R' - R) \\ &+ \phi^I(R)A^{-1} \phi^I(R')\Theta(R - R'), \end{aligned} \quad (C24)$$

where Θ is the Heaviside step function and M is a constant matrix computed from the expression

$$A = \phi^I(R)^T \frac{d}{dR} \phi^R(R) - \phi^I(R)^T \frac{d}{dR} \phi^R(R). \quad (C25)$$

Even though this expression is seemingly dependent of R , A is a constant matrix (see Ref. [47] for details) and can be evaluated at an arbitrary point R . One of the advantages of this approach is the relative simplicity of obtaining the set of solutions. Solutions can be calculated by simply integrating from the boundary conditions outward/inward, which can be done over long distances. This allows us to construct Green's function even for long-range potentials on a grid.

-
- [1] M. Zawadzki, M. Čížek, K. Houfek, R. Čurík, M. Ferus, S. Civiš, J. Kočíšek, and J. Fedor, Resonances and dissociative electron attachment in HNCO, *Phys. Rev. Lett.* **121**, 143402 (2018).
- [2] Ragesh Kumar T. P., P. Nag, M. Ranković, R. Čurík, A. Knížek, S. Civiš, M. Ferus, J. Trnka, K. Houfek, M. Čížek, and J. Fedor, Electron-impact vibrational excitation of isocyanic acid HCNO, *Phys. Rev. A* **102**, 062822 (2020).
- [3] I. Zinchenko, C. Henkel, and R. Q. Mao, HNCO in massive galactic dense cores, *Astronom. Astrophys.* **361**, 1079 (2000).
- [4] D. C. Lis, J. Keene, K. Young, T. G. Phillips, D. Bocklee-Morvan, J. Crovisier, P. Schilke, P. F. Goldsmith, and E. Bergin, Spectroscopic observations of comet C/1996 B2 (Hyakutake) with the Caltech submillimeter observatory, *Icarus* **130**, 355 (1997).
- [5] G. Fedoseev, S. Ioppolo, D. Zhao, T. Lamberts, and H. Linnartz, Low-temperature surface formation of NH₃ and HNCO: hydrogenation of nitrogen atoms in CO-rich interstellar ice analogues, *Mon. Not. R. Astron. Soc.* **446**, 439 (2015).
- [6] L. Song and J. Kastner, Formation of the prebiotic molecule NH₂CHO on astronomical amorphous solid water surfaces: Accurate tunneling rate calculations, *Phys. Chem. Chem. Phys.* **18**, 29278 (2016).
- [7] T. P. Ragesh Kumar, P. Nag, M. Rankovic, T. F. M. Luxford, J. Kočíšek, Z. Mašín, and J. Fedor, Distant symmetry control in electron-induced bond cleavage, *J. Phys. Chem. Lett.* **13**, 11136 (2022).
- [8] I. I. Fabrikant, S. Eden, N. J. Mason, and J. Fedor, Recent progress in dissociative electron attachment: From diatomics to biomolecules, *Adv. At. Mol. Opt. Phys.* **66**, 545 (2017).
- [9] G. A. Gallup, P. D. Burrow, and I. I. Fabrikant, Electron-induced bond breaking at low energies in HCOOH and glycine: The role of very short-lived σ^* anion states, *Phys. Rev. A* **79**, 042701 (2009).
- [10] T. N. Rescigno, C. S. Trevisan, and A. E. Orel, Dynamics of low-energy electron attachment to formic acid, *Phys. Rev. Lett.* **96**, 213201 (2006).
- [11] C. H. Yuen, N. Douguet, S. Fonseca dos Santos, A. E. Orel, and V. Kokoouline, Simplified model to treat the electron attachment of complex molecules: Application to H₂CN and the quest for the CN⁻ formation mechanism, *Phys. Rev. A* **99**, 032701 (2019).
- [12] T. N. Rescigno, C. S. Trevisan, A. E. Orel, D. S. Slaughter, H. Adaniya, A. Belkacem, M. Weyland, A. Dorn, and C. W. McCurdy, Dynamics of dissociative electron attachment to ammonia, *Phys. Rev. A* **93**, 052704 (2016).
- [13] N. Douguet, D. S. Slaughter, H. Adaniya, A. Belkacem, A. E. Orel, and T. N. Rescigno, Signatures of bond formation and bond scission dynamics in dissociative electron attachment to methane, *Phys. Chem. Chem. Phys.* **17**, 25621 (2015).
- [14] M. Tarana, K. Houfek, J. Horáček, and I. I. Fabrikant, Dissociative electron attachment and vibrational excitation of CF₃Cl: Effect of two vibrational modes revisited, *Phys. Rev. A* **84**, 052717 (2011).
- [15] D. J. Haxton, Z. Zhang, H.-D. Meyer, T. N. Rescigno, and C. W. McCurdy, Dynamics of dissociative attachment of electrons to water through the ²B₁ metastable state of the anion, *Phys. Rev. A* **69**, 062714 (2004).
- [16] D. J. Haxton, T. N. Rescigno, and C. W. McCurdy, Dissociative electron attachment to the H₂O molecule. II. Nuclear dynamics on coupled electronic surfaces within the local complex potential model, *Phys. Rev. A* **75**, 012711 (2007).
- [17] S. T. Chourou and A. E. Orel, Dissociative electron attachment to HCN and HNC, *Phys. Rev. A* **80**, 032709 (2009).
- [18] S. T. Chourou and A. E. Orel, Isotope effect in dissociative electron attachment to HCN, *Phys. Rev. A* **83**, 032709 (2011).
- [19] W. Domcke, Theory of resonance and threshold effects in electron-molecule collisions: The projection-operator approach, *Phys. Rep.* **208**, 97 (1991).
- [20] W. Domcke and L. S. Cederbaum, Vibration-induced narrowing of electron scattering resonances near threshold, *J. Phys. B: At. Mol. Phys.* **13**, 2829 (1980).
- [21] L. S. Cederbaum and W. Domcke, Local against non-local complex potential in resonant electron-molecule scattering, *J. Phys. B: At. Mol. Phys.* **14**, 4665 (1981).
- [22] W. Domcke and L. S. Cederbaum, On the interpretation of low-energy electron-HCl scattering phenomena, *J. Phys. B: At. Mol. Phys.* **14**, 149 (1981).
- [23] M. Čížek, J. Horáček, and W. Domcke, Nuclear dynamics of the H₂⁻ collision complex beyond the local approximation: Associative detachment and dissociative attachment to rotationally and vibrationally excited molecules, *J. Phys. B: At. Mol. Opt. Phys.* **31**, 2571 (1998).
- [24] M. Čížek and K. Houfek, Nonlocal Theory of Resonance Electron-Molecule Scattering, in *Low-energy Electron Scattering from Molecules, Biomolecules and Surfaces*, edited by P. Čársky and R. Čurík (CRC Press, Boca Raton, 2012), Chap. 4, pp. 91–125.

- [25] J. Horáček, M. Čížek, K. Houfek, P. Kolorenč, and W. Domcke, Dissociative electron attachment and vibrational excitation of H₂ by low-energy electrons: Calculations based on an improved nonlocal resonance model, *Phys. Rev. A* **70**, 052712 (2004).
- [26] C. S. Trevisan, K. Houfek, Z. Zhang, A. E. Orel, C. W. McCurdy, and T. N. Rescigno, Nonlocal model of dissociative electron attachment and vibrational excitation of NO, *Phys. Rev. A* **71**, 052714 (2005).
- [27] M. Čížek, J. Horáček, A. Ch. Sergenton, D. B. Popovic, M. Allan, W. Domcke, T. Leininger, and F. Gadea, Inelastic low-energy electron collisions with the HBr and DBr molecules: Experiment and theory, *Phys. Rev. A* **63**, 062710 (2001).
- [28] H. Estrada, L. S. Cederbaum, and W. Domcke, Vibronic coupling of short-lived electronic states, *J. Chem. Phys.* **84**, 152 (1986).
- [29] H. B. Ambalampitiya and I. I. Fabrikant, Nonlocal complex potential theory of dissociative electron attachment: Inclusion of two vibrational modes, *Phys. Rev. A* **102**, 022802 (2020).
- [30] J. Dvořák, M. Ranković, K. Houfek, P. Nag, R. Čurík, J. Fedor, and M. Čížek, Vibronic coupling through the continuum in the $e+\text{CO}_2$ system, *Phys. Rev. Lett.* **129**, 013401 (2022).
- [31] J. Dvořák, K. Houfek, and M. Čížek, Vibrational excitation in the $e+\text{CO}_2$ system: Nonlocal model of Σ - Π vibronic coupling through the continuum, *Phys. Rev. A* **105**, 062821 (2022).
- [32] J. Dvořák, M. Ranković, K. Houfek, P. Nag, R. Čurík, J. Fedor, and M. Čížek, Vibrational excitation in the $e+\text{CO}_2$ system: Analysis of the two-dimensional energy-loss spectrum, *Phys. Rev. A* **106**, 062807 (2022).
- [33] C. Glidewell and C. Thomson, Basis set dependence of the barrier to linearity in HNCO, *Chem. Phys. Lett.* **104**, 287 (1983).
- [34] M. Čížek, J. Horáček, M. Allan, and W. Domcke, Resonances and threshold phenomena in low-energy electron collisions with hydrogen halides: New experimental and theoretical results, *Czech. J. Phys. B* **52**, 1057 (2002).
- [35] J. Fedor, C. Winstead, V. McKoy, M. Čížek, K. Houfek, P. Kolorenč, and J. Horáček, Electron scattering in HCl: An improved nonlocal resonance model, *Phys. Rev. A* **81**, 042702 (2010).
- [36] P. Knowles, C. Hampel, and H. Werner, Coupled-cluster theory for high-spin, open-shell reference wave-functions, *J. Chem. Phys.* **99**, 5219 (1993).
- [37] M. J. O. Deegan and P. J. Knowles, Perturbative corrections to account for triple excitations in closed and open-shell coupled-cluster theories, *Chem. Phys. Lett.* **227**, 321 (1994).
- [38] T. H. Dunning, Gaussian-basis sets for use in correlated molecular calculations. 1. The atoms boron through neon and hydrogen, *J. Chem. Phys.* **90**, 1007 (1989).
- [39] H.-J. Werner, P. J. Knowles *et al.*, MOLPRO, version 2012, a package of *ab initio* programs, see <https://www.molpro.net>.
- [40] Z. Mašín, J. Benda, J. D. Gorfinkiel, A. G. Harvey, and J. Tennyson, UKRmol+: A suite for modelling electronic processes in molecules interacting with electrons, positrons and photons using the *R*-matrix method, *Comput. Phys. Commun.* **249**, 107092 (2020).
- [41] J. Tennyson, Electron–molecule collision calculations using the *R*-matrix method, *Phys. Rep.* **491**, 29 (2010).
- [42] H.-D. Meyer, J. Horáček, and L. S. Cederbaum, Schwinger and anomaly-free Kohn variational principles and a generalized Lanczos algorithm for nonsymmetric operators, *Phys. Rev. A* **43**, 3587 (1991).
- [43] M. Allan, M. Čížek, J. Horáček, and W. Domcke, Electron scattering in cooled HCl: Boomerang structures and outer-well resonances in elastic and vibrational excitation cross sections, *J. Phys. B: At., Mol. Opt. Phys.* **33**, L209 (2000).
- [44] J. Dvořák, Contribution to theory of low-energy electron-molecule collisions, Ph.D. thesis, Charles University, 2023.
- [45] M. Čížek, J. Horáček, and H. D. Meyer, Schwinger-Lanczos algorithm for calculation of off-shell *T*-matrix elements and Wynn's epsilon algorithm, *Comput. Phys. Commun.* **131**, 41 (2000).
- [46] W. Domcke and C. Mündel, Calculation of cross sections for vibrational excitation and dissociative attachment in HCl and DCl beyond the local-complex-potential approximation, *J. Phys. B: At. Mol. Phys.* **18**, 4491 (1985).
- [47] D. L. Foulis, Partial-wave Green-function expansions for general potentials, *Phys. Rev. A* **70**, 022706 (2004).
- [48] M. Čížek, Resonant processes in atomic collisions, theoretical considerations and calculations, Ph.D. thesis, Charles University, 1999.